Proceedings of the ASME 2020
14th International Conference on Energy Sustainability
ES2020
June 8-10, 2020, Denver, CO, USA

ES2020-9555

IMAGING PARTICLE TEMPERATURES AND CURTAIN OPACITIES USING AN IR CAMERA

Jesus D. Ortega[1], Guillermo Anaya, Peter Vorobieff, Gowtham Mohan
University of New Mexico
Albuquerque, NM, USA

Clifford K. Ho
Sandia National Laboratories
Albuquerque, NM, USA

ABSTRACT

The Falling Particle Receiver (FPR) at the National Solar Thermal Test Facility (NSTTF) is one of the central receiver technologies which offers a solution to the temperature and irradiance limitations exhibited by gas and molten salt receivers, since the particle curtain is directly irradiated without the need of containment. Nonetheless, the heat loss characterization of the 1 MWth FPR has been a feat which is still not fully addressed. One of the challenges of the FPR characterization is the intricate flow conditions that the particle curtain experiences due to its cavity design with a single aperture, to allow the direct irradiance, that does not have a window. Recently, particle plumes that were expelled from the FPR during operation were observed. While this is phenomenon that needs to be closely monitored, it is extremely difficult to operate any kind of sensors near the aperture of the FPR. This work describes the development of a methodology using a high-speed IR camera, located ≥5 meters away from the aperture, to estimate the opacity of a particle plume, which in turn can be used to extract the average particle temperature of a region of interest with a known background temperature. Experiments performed at the University of New Mexico using 4 different flow configurations and 3 different temperatures (200, 450, and 750°C) were perform to investigate the relationship between the plume opacity, on the visible range, and the "particle-pixel" opacity, obtained from the thermograms. The "particle-pixel function" is a relationship that describes the combined impact of an unknown number of particles, at a specific temperature, on a thermogram pixel with initial value equal to the background temperature. The novelty of this function is that it provides a reasonable estimate of the plume opacity using thermograms obtained from the IR camera; hence a bulk particle temperature can be obtained. Future work for this methodology will consist on completing the methodology to compute the advective losses from the FPR and provide a first order approximation of the convective losses for the system.

Keywords: Falling Particle Receiver, Advective Losses, Imaging Methods

NOMENCLATURE

The following nomenclature is used throughout this work:

Variables

$\dot{m}$	Mass flow rate (g/s)
A_f	Flow area (mm^2)
ρ	Density (g/cm^3)
V	Velocity (m/s)
ω	Opacity
φ	Volume fraction
D	Diameter (mm)
τ	Curtain thickness (mm)
ϵ	Emissivity
T	Temperature (C or K)
C_p	Specific heat capacity (J/kg-K)
h	Enthalpy (J/kg)

Subscripts

a	Air
p	Particle
px	Pixel
bk	Background
b	Bulk
out	Flowing out of the system
in	Flowing into the system

INTRODUCTION

A particle receiver is a type of concentrating solar power (CSP) receiver which is currently being pursued to enable higher temperatures (>700 °C) which can yield greater power cycle efficiencies (≥50%) [1]. These systems use sub-millimeter size particles which fall through a receiver and are directly heated by a beam of concentrated sunlight. Once the particles reach a desired temperature, they can be stored and used when needed for electricity production, process heating, thermochemistry, or solar-fuel production. Sandia National Laboratories has previously demonstrated a 1 MWth high-temperature falling particle receiver system that has achieved

[1] Contact author: jdortega4@unm.edu

particle temperatures over 700 °C [2-4]. The ceramic particles (from CARBO Ceramics) are composed of sintered bauxite and are ~350 microns in diameter. During this study, the Sandia team found that during operation, smoke-like plumes were emitted from the aperture as seen on Figure 1. It was later found that these plumes were composed of particles that were expelled from the receiver aperture. Since advective losses contribute to the heat losses from the system (convective and radiative), quantifying the amount of mass and energy losses is paramount to reduce heat and particle losses which are needed to increase receiver thermal efficiencies and reduce O&M costs. This paper summarizes imaging methods to characterize the particle temperature and opacity of the plumes.

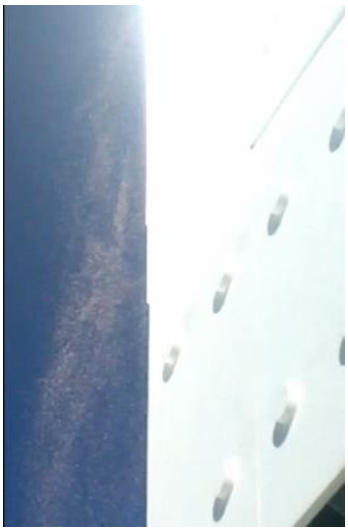

Figure 1. Particle plumes observed during FPR testing.

METHODOLOGY

The main challenge of this project is to develop a methodology which is able to provide accurate measurements of mass and energy losses with a fixed constraint of placing the devices being used at least 5 meters away from the receiver aperture to avoid direct exposure from the concentrated sunlight incident on the receiver. Due to this constraint, camera-based methodologies were assessed to identify the ideal method to perform in-situ measurements of particle loss from the falling particle receiver (FPR).

For this study, five methodologies were considered and their advantages or disadvantages are listed below. In order to assess the potential of these methods, a small particle receiver (SPR) was built at the University of New Mexico (UNM) which operates analogously to the FPR at Sandia National Labs; however, the particle curtain mass flow rates correspond to those estimated for the particle losses experienced by the FPR. As seen in Figure 2, the experimental setup is comprised of an actuated tube furnace, a solar simulator and an SPR. To capture the experimental data, the SPR has been equipped with thermocouples in the top and bottom hoppers, along with a ± 0.5 gram resolution scale, to record particle temperature and mass change data as the images are captured by the three cameras as shown in Figure 3 and Figure 4.

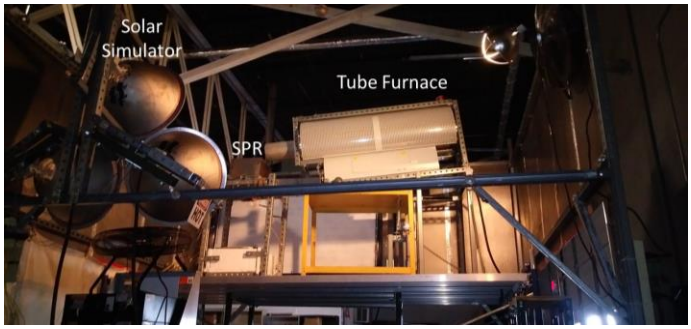

Figure 2. Experimental Setup at UNM

Figure 3. InfraTec thermographic system ImageIR® 8320 HP with 100 mm lens is used to record the thermograms from the SPR from the front view.

Figure 4. A Nikon D3500 and a Logitech C920 were used to capture images from the front and side views of the curtain.

Theory

To estimate the advective heat losses ($\dot{Q}_{loss}$), the particle temperature and mass flow rate must be known as shown in Eq. 1 [5]. Therefore, the method selected must be able to provide inputs to estimate the mass flow rate and particle temperatures since the focus of this work is to obtain the correct estimates for the particles part only. These values can be obtained from Eq. 2 and Eq. 3.

$$\dot{Q}_{loss} = \dot{m}_p \overline{C_p}\left(T_{p,out} - T_{p,in}\right) + \dot{m}_a\left(h_{a,out} - h_{a,in}\right) \quad (1)$$

$$\dot{m}_p = \rho_b A_f V_p \quad (2)$$

$$\epsilon_{px} T_{px}^4 = \epsilon_p \omega T_p^4 + (1-\omega)\epsilon_{bk} T_{bk}^4 \quad (3)$$

For these two equations, there are three unknown values, the bulk density of the particles, the particle temperature, and the opacity of the curtain; thus, an ill-posed problem. Opacity and bulk density can be related by using the modified version of Beer's law in Eq. 4, and the particle volume fraction relationship in Eq. 5 into a single equation (Eq. 6) [6]. Lastly, the particle temperature can be found from the thermograms by rearranging the energy equation (Eq. 2) and turning it into Eq. 7. From here it can be seen that both bulk density and particle temperature are function of curtain opacity which is an unknown.

$$\omega = 1 - e^{-\frac{3\varphi_p \tau}{2D_p}} \quad (4)$$

$$\varphi_p = \frac{\rho_b}{\rho_p} \quad (5)$$

$$\rho_b = -\frac{2D_p \rho_p}{3\tau} \ln(1-\omega) \quad (6)$$

$$T_p = \left(\frac{\epsilon_{px} T_{px}^4 - (1-\omega)\epsilon_{bk} T_{bk}^4}{\epsilon_p \omega}\right)^{1/4} \quad (7)$$

Experimental Methodologies

The following subsections describe the five methods considered to eliminate the ill-posed nature of the problem.

Method 1: Experimental Calibrations

For this method, a large experimental calibration matrix will need to be developed in order to build a database of thermograms and flow conditions similar to those experienced by the expelled particles on the FPR. This method requires to perform a large matrix of experiments to generate some form of experimental calibration using the thermograms only. In the lab-scale experiments, the mass flow rate was measured and recorded thermogram sets to estimate the cross-sectional flow area and the particle velocity to get an estimate of particle bulk density. Using the bulk density and curtain thickness the curtain opacity can be estimated as well as the particle temperature from the measured pixel temperature, background temperature, and opacity. However, this method requires a large set of experiments with variable mass flow, curtain thickness, and temperatures to generate calibration factors to adjust the temperature ranges. The set of lab-scale experiments may not cover all the conditions during the on-sun tests.

Method 2: Particle Temperature Estimate

This method requires an estimate of the temperature of the particles expelled from the cavity using measured inlet and outlet particle temperatures as inputs. Having an estimate of the particle temperature, we can obtain the plume opacity from the energy equation (Eq. 3) and the recorded pixel temperatures from the thermograms. From the opacity and plume thickness measurement we can obtain the particle volume fraction; hence, the bulk density. Knowing the bulk density, the flow area, and the plume velocity from the thermograms, we obtain the mass flow rate. This mass flow rate can be validated with the mass flow measurements done. While this method sounds reasonable, the particle temperature is only an estimate based on the measured temperatures through the system thermocouples and not the cameras.

Method 3: IR Camera with Particle-Pixel Function

Estimating the curtain opacity directly from the IR camera measurements would be ideal. Perhaps this could be done by means of a particle-pixel function (PPF) that would be used to correlate particle to pixel temperatures without using the opacity as a variable as in Eq. 3. Using the PPF, the particle temperature could be estimated directly from the thermograms. By obtaining the particle temperature from the pixel temperature, the average curtain opacity can be estimated from the energy equation (Eq. 3) for selected subsections throughout the curtain. From the average opacity and plume thickness measurement the particle volume fraction can be obtained as well as the bulk density. Knowing the bulk density, the flow area, and the plume velocity from the thermograms, the mass flow rate can be estimated. This methodology was further tested and the results are presented in the next section.

Method 4: Visible and IR Camera Combination

Introducing a front-view visible-light camera in combination with the IR camera, and visualizing the same field of view, the curtain opacity can be estimated much more accurately. Using this camera, the curtain opacity values can be extracted from the visible-light images, by selecting sub-regions within the curtain. These regions in the visible-light images can be then matched to the sub-regions on the thermograms, to estimate average pixel temperatures. Average pixel temperatures combined with the average opacity of selected sub-regions, can be used to extract the particle temperature Moreover, from the opacity and plume thickness measurement the particle volume fraction and the bulk density can be estimated. Knowing the bulk density, the flow area, and the plume velocity from the thermograms, the mass flow rate can also be obtained.

Method 5: IR Camera with Emissivity Calibration

Using this methodology entails calibrating the emissivity of the camera to match particle temperatures to measured pixel temperatures. Similar to Method 1, the lab-scale experiments can be used to determine a correlation between camera emissivity and parameters, such as background temperature and curtain opacity. In this case, the emissivity value

becomes the calibration factor to get the particle temperature from pixel temperature. This makes it possible to determine the correlation between this multiplier and the opacity. However, this calibration factor is a function of the curtain opacity, temperature, or other parameters that requires numerous tests spanning the range of possible conditions.

Methodology Selection

Because of the large subset of experiments needed to capture a significant number of cases that could occur during the on-sun tests, we decided that Method 1 and 5 would not be considered any further. Moreover, in the case of Method 5, having to change the effective emissivity value, in the IR camera, every measurement to capture a better estimate of the particle temperature would be a tedious task since the variation of effective emissivity will be directly correlated to the particle temperature and opacity. This is unreliable as the results would be based on a qualitative analysis to capture the data used to calculate the results. In the case of Method 2, since the initial particle temperature used in the analysis would be an estimate based on the inlet/outlet particle temperatures of the receiver, we also decided against further consideration, unless it was necessary.

Accordingly, we decided to pursue our two remaining options: Method 3, using the IR camera only and deriving a particle-pixel function which could decouple the particle temperature and opacity of the curtain, and Method 4, which would introduce a visible-light camera to quantify the opacity, making it possible to estimate the particle temperature of the curtain.

EXPERIMENTAL RESULTS

While assessing these methods, a sensitivity and variable correlation study was performed using the independent variables found in the energy equation (Eq. 3). A set of analytical cases were generated using Eq. 2 through Eq. 4. The study revealed that while the background temperature is kept constant, the influences of particle temperature and the particle mass flow rate, which directly impacts the opacity, on the pixel temperature could not be easily decoupled. In the variable correlation study, we generated 460 cases using 23 temperatures from 200ºC to 750ºC in increments of 25ºC and 10 mass flow rates between 0.6 to 6 g/s. The results of this study, displayed in Table 2, show that while the particle temperature shows a higher correlation to the pixel temperature than the mass flow rate, both values show a positive correlation value above 50%.

Table 1. Variable correlation study using the 460 cases generated. Values closer to -1 represent a negative correlation, while values closer to 1 represent a positive correlation.

Variable Correlation Study

	$T_p(C)$	$\dot{m}_b$ (g/s)	$T_{px}(C)$
T_p (C)	1		
$\dot{m}_b$ (g/s)	0.0000	1	
T_{px} (C)	0.8169	0.5073	1

To compare both remaining methods, we performed three experiments with average flow rate of ~6 g/s (20 kg/h) and three temperatures (200, 450, 750ºC). During the experiments, thermogram sets, and front and side view images were recorded using the IR and visible-light cameras.

Method 3: IR Camera with Particle-Pixel Function

The key feature of this method is that it correlates the particle and pixel temperatures through a function which does not include an opacity as a variable. The development of the particle-pixel function (PPF) was done using the three experiments aforementioned.

First, the thermogram sets are imported into MATLAB and a region of interest is selected to reduce the computational domain and eliminate the background temperatures as seen in Figure 5. For this region the average pixel temperature can be extracted as a function of flow position, as seen in Figure 6. Similarly, the average particle temperature as a function of position can be found by fitting the temperatures measured by the thermocouples mounted on the top and bottom hoppers with the lumped capacitance model (LCM), as seen in Figure 6.

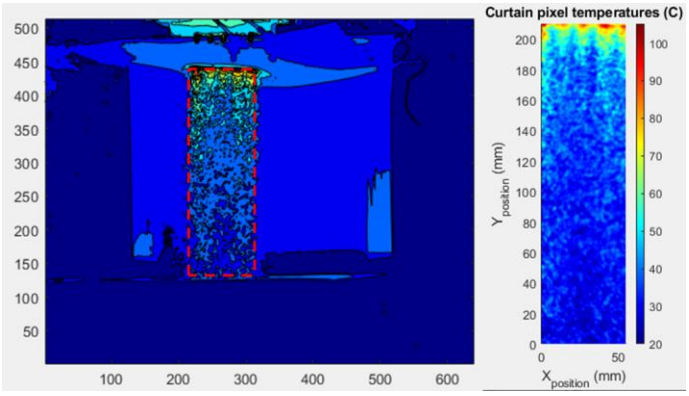

Figure 5. A set of thermograms is imported into MATLAB and a region of interest (ROI) is selected. This ROI is used throughout the calculations.

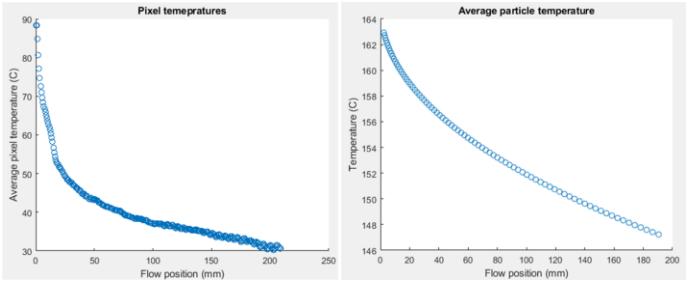

Figure 6. Average pixel temperature extracted from the ROI (left) and average particle temperature fitted by the lumped capacitance model (right) as a function of flow position.

Figure 7 shows that the average particle and pixel temperatures are not proportional and since the ranges vary, the data is difficult to collapse onto a master curve. Nevertheless, by restructuring the data, a curve fit with an R=0.993 was achieved to correlate the data of the three experiments as shown in Figure

8. In Figure 9, we can see how the PPF can be used to estimate the particle temperatures.

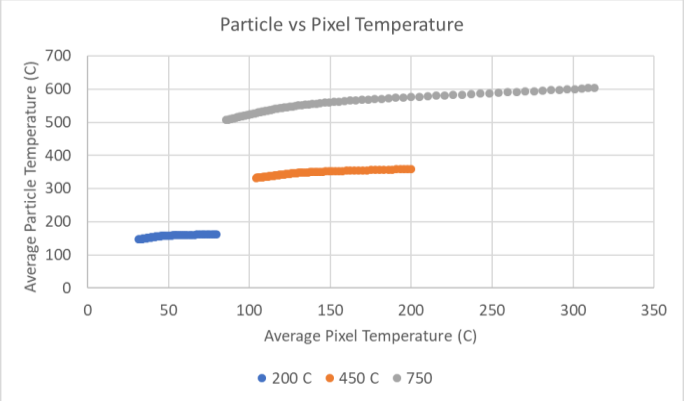

Figure 7. The average particle temperature is not proportional to the average pixel temperature for tests at different temperatures.

Using the particle-pixel function, a previous set of experiments of this project was analyzed. If the PPF can predict the correct particle temperature using the pixel temperatures measured in the different cases, then the PPF is independent of mass flow rate and opacity, and the function is applicable to any experiment. If successful, these particle temperature estimates can be used to calculate the opacity of the curtain using the energy equation (Eq. 3). If it fails, it means that the pixel temperatures are heavily dependent on both opacity and particle temperature, which will require knowing the opacity beforehand in order to calculate the particle temperatures.

Unfortunately, while the cases with a flow rate similar to the one used to develop the particle-pixel function seem to correlate the particle and pixel temperatures very well, for the cases with lower mass flow rates, the PPF failed to predict the correct particle temperatures. This is a likely manifestation of the intricate correlation between particle temperature, mass flow rate, and pixel temperature. It was decided to move to Method 4 which uses a visible-light camera to estimate the opacity of the curtain at the same time as the IR camera records the pixel temperatures.

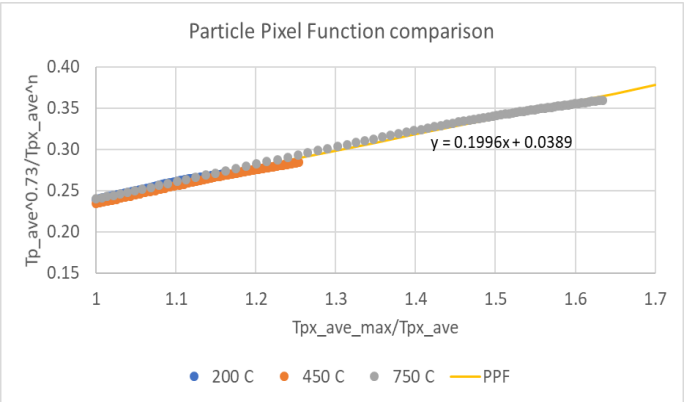

Figure 8. Correlation of measured particle temperatures to particle pixel temperature for a subset of tests.

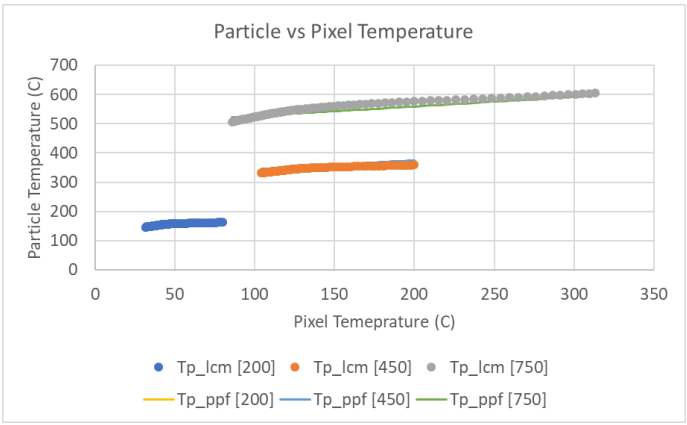

Figure 9. Estimated particle temperature using the PPF and the average pixel temperature for a mass flow rate of ~6 g/s, similar to the mass flow rate used in the determination of the PPF.

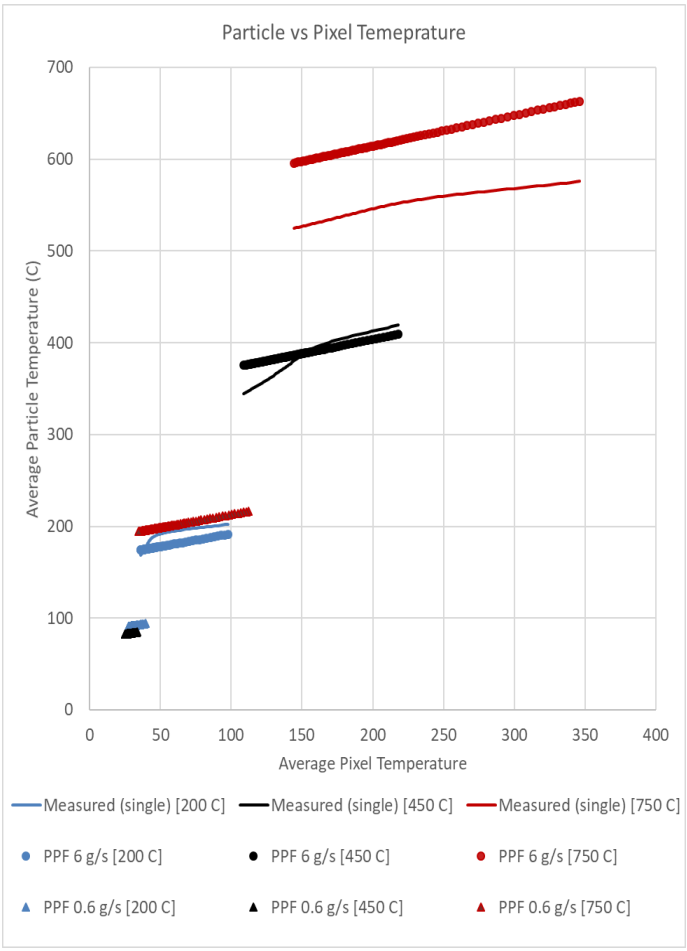

Figure 10. Estimated particle temperature using the PPF and the average pixel temperature for mass flow rates of ~6 g/s and 0.6 g/s.

Method 4: Visible and IR Camera Combination

Since Method 3 showed a strong dependency of pixel temperature on particle temperature and mass flow rate, a visible-light camera was installed to capture images of the curtain in order to estimate the opacity as seen in Figure 4. To

achieve this, a Nikon D3500 will be taking synchronized snapshots with the IR camera as shown in Figure 11.

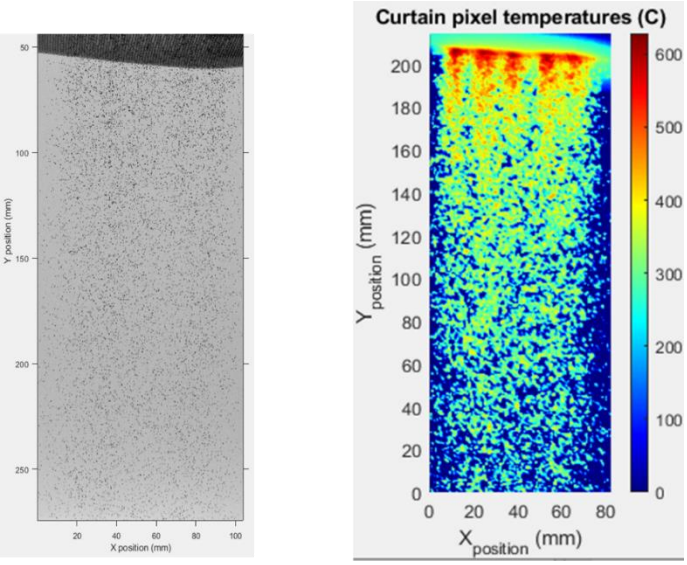

Figure 11. ROI of Visible images (left) captured simultaneously with the IR camera thermograms recorded with a calibration range of 125-300ºC (right).

The procedure to compute the opacity is straightforward:

- Convert the NEF image file to TIFF
    - 48-bit for RGB (16-bit each)
- MATLAB Code reads 1st image
- Code prompts to select 2 points for calibration
- Code prompts to select Region of Interest (ROI)

Once the analysis settings are set for the first image, the code imports the rest of the sequence of images. To perform the analysis the opacity was calculated in three regions throughout the curtain, as shown in Figure 12**Error! Reference source not found.**. The sections are binarized to convert the greyscale image into a black-and-white image shown in Figure 13. The binary images can be used to estimate the opacity of the three sections (Figure 14). From the thermograms, the average pixel temperatures of the same regions (Figure 15) can be extracted and using the average opacity of the region, the average particle temperature can be estimated using the energy equation (Eq. 3).

Lastly, to validate the methodology, the average particle temperature extracted was compared with the empirically derived particle temperatures from the lumped capacitance exponential fits as seen in Figure 16. Current results show that the average particle temperatures extracted using this methodology can yield temperatures with an error below 10% from the empirical value of the LCM curve.

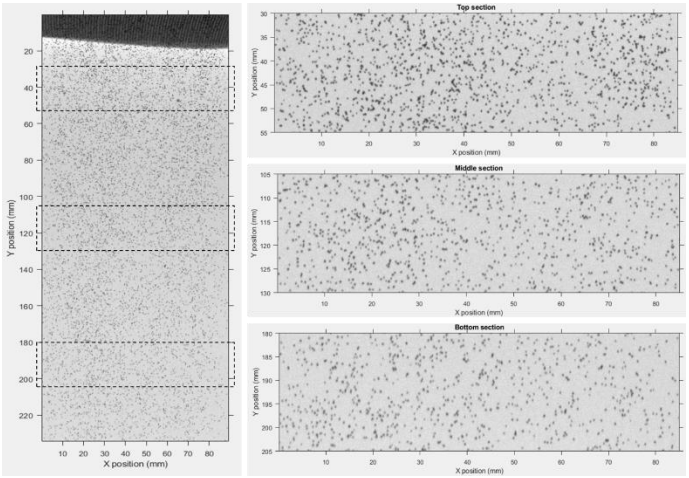

Figure 12. To estimate the opacity of the curtain, three regions were selected in the top, middle and bottom parts within the curtain to be analyzed.

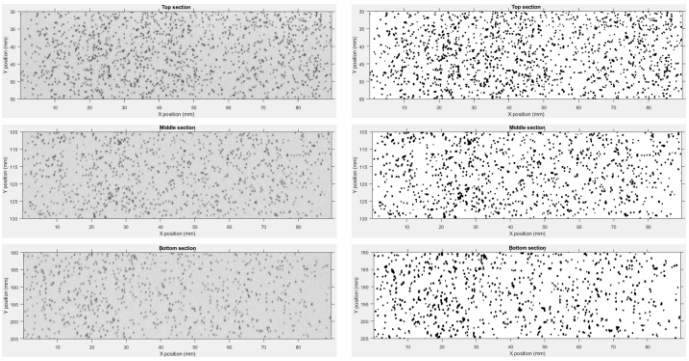

Figure 13. Sections get binarized using *imbinarize* function in MATLAB.

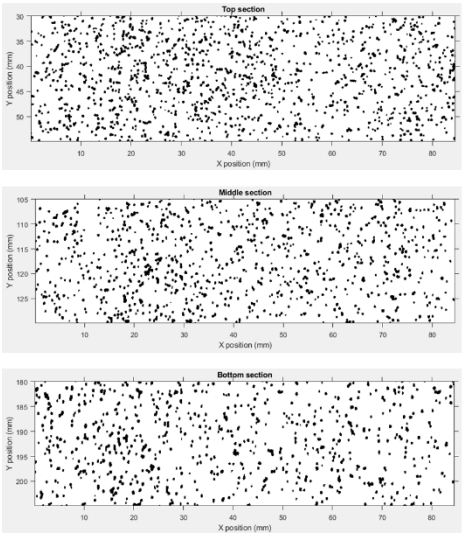

$\bar{\omega} = 0.1094 \pm 0.0024$

$\bar{\omega} = 0.0874 \pm 0.0032$

$\bar{\omega} = 0.0779 \pm 0.0022$

Figure 14. Opacity estimation results using binary images.

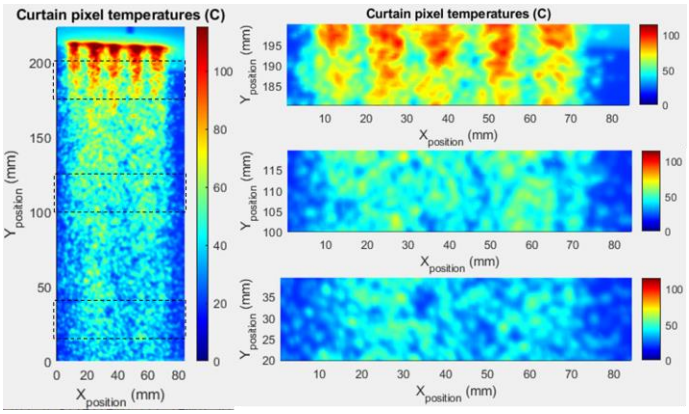

Figure 15. The thermograms are divided into three similar sections and used to get the average particle temperature using the average pixel temperature and measured opacity.

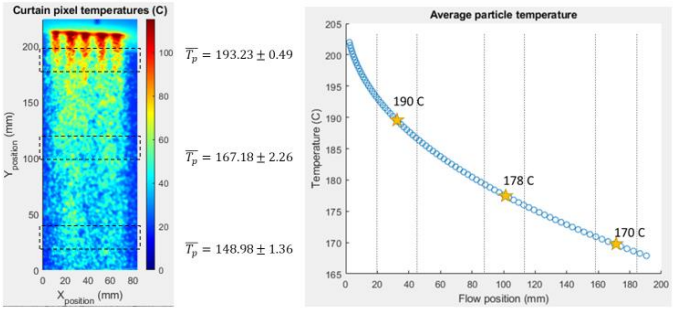

Figure 16. Comparison of particle temperature extracted from energy equation when knowing the opacity and pixel temperature (left) and empirical temperature curve based on the lumped capacitance method (right).

CONCLUSION

As this methodology is applied to the results obtained previously in the project, Method 4 has proven to yield the best results so far. The average particle temperatures within the sub-regions are shown to be close to the ±10% error which will enable the estimation of the mass and energy flows of the particles. Lastly, there are two main valuable lessons learned for future experiments to continue streamlining this methodology.

1. The IR camera calibration temperature range is important to get valuable pixel temperatures. This is extremely important because when the measured pixel temperatures go outside of the selected range, the temperature difference error becomes more prominent. Looking back to Figure 16, where the selected camera range was 125-300°C, the particle move downstream, the pixel temperature deviates farther from the range, and this can lead to lower pixel values than those expected is a lower pixel range was chosen (e.g., 30-150°C).
2. The visible camera settings are extremely important for consistency as the repeatability. As the curtain images are recorded, it is important to have a constant reference since the *imbinarize* function in MATLAB uses this reference intensity value (close to 65535 for white and 0 for black pixels 16-bit images) while the pixels that resolve the particles have a value which is far lower than the reference. This is not trivial as this conversion is crucial to estimate the curtain opacity accurately.

ACKNOWLEDGEMENTS

The authors thank Matthew Bauer and Andru Prescod from DOE for their management and support of this work, which was funded by DOE's Solar Energy Technologies Office (Gen 3 Lab Call). Sandia National Laboratories is a multimission laboratory managed and operated by National Technology and Engineering Solutions of Sandia, LLC., a wholly owned subsidiary of Honeywell International, Inc., for the U.S. Department of Energy's National Nuclear Security Administration under contract DE-NA0003525.

REFERENCES

[1] C.K. Ho, 2016, A Review of High-Temperature Particle Receivers for Concentrating Solar Power, *Applied Thermal Engineering*, 109(Part B), p. 958-969.

[2] C.K. Ho, J.M. Christian, J. Yellowhair, K. Armijo, and S. Jeter, 2016, *Performance Evaluation of a High-Temperature Falling Particle Receiver*, *ASME Power & Energy Conference*, Charlotte, NC, June 26-30, 2016.

[3] C.K. Ho, J.M. Christian, J. Yellowhair, S. Jeter, M. Golob, C. Nguyen, K. Repole, S.I. Abdel-Khalik, N. Siegel, H. Al-Ansary, A. El-Leathy, and B. Gobereit, 2017, *Highlights of the High-Temperature Falling Particle Receiver Project: 2012 - 2016*, in *SolarPaces 2016: International Conference on Concentrating Solar Power and Chemical Energy Systems*, Abu Dhabi, UAE, October 11 - 14, 2016.

[4] C.K. Ho, J.M. Christian, J. Yellowhair, N. Siegel, S. Jeter, M. Golob, S.I. Abdel-Khalik, C. Nguyen, and H. Al-Ansary, 2016, On-Sun Testing of an Advanced Falling Particle Receiver System, *Solarpaces 2015: International Conference on Concentrating Solar Power and Chemical Energy Systems*, 1734.

[5] C.K. Ho, J.D. Ortega, V. Martins, S. Kinahan, P. Vorobieff, A.A. Mammoli, 2019, *Characterization of Particle and Heat Losses from a Falling Particle Receiver*, *ASME Energy Sustainability Conference*, Bellevue, WA, July 15-17, 2019.

[6] Kim, K., N. Siegel, G. Kolb, V. Rangaswamy, and S.F. Moujaes, 2009, A study of solid particle flow characterization in solar particle receiver, *Solar Energy*, 83(10), p. 1784-1793.